

Hydrodynamical simulations of convection-related stellar micro-variability

I. Statistical relations for photometric and photocentric variability

Hans-Günter Ludwig^{1,2}

¹ Lund Observatory, Lund University, Box 43, 22100 Lund, Sweden

² GEPI, CIFIST, Observatoire de Paris-Meudon, 5 place Jules Janssen, 92195 Meudon Cedex, France
e-mail: Hans.Ludwig@obspm.fr

Received date; accepted date

Abstract. Local-box hydrodynamical model atmospheres provide statistical information about the spatial dependence, as well as temporal evolution, of a star’s emergent radiation field. Here, we consider late-type stellar atmospheres for which temporal changes of the radiative output are primarily related to convective (granular) surface flows. We derived relations for evaluating the granulation-induced, disk-integrated thus observable fluctuations of the stellar brightness and location of the photocenter from radiation intensities available from a local model. Apart from their application in the context of hydrodynamical stellar atmospheres, these formulae provide some broader insight into the nature of the fluctuations under consideration. Brightness fluctuations scale inversely proportional to the square root of the number of convective cells (the statistically independently radiating surface elements) present on the stellar surface and increase with more pronounced limb-darkening. Fluctuations of the stellar photocentric position do *not* depend on the number of cells and are largely insensitive to the degree of limb-darkening. They amount to a small fraction of the typical cell size, and can become a limiting factor for high-precision astrometry in the case of extreme giants. The temporal brightness and positional fluctuations are statistically uncorrelated but closely related in magnitude.

Key words. convection – hydrodynamics – radiative transfer – methods: numerical – stars: atmospheres – stars: late-type

1. Introduction

The presence of granular flows on the surfaces of late-type stars implies ultimate limits to their photometric stability, the stability of the position of their photometric centroid (hereafter “photocenter”), and the stability of their spectroscopically determined radial velocities. The searches for extrasolar planets and stellar p-mode oscillations have been pushing towards higher observational sensitivity, now allowing the detection of the low-level (hence “micro-”) variability induced by the stochastically changing granular flow pattern (e.g., Kjeldsen et al. 1999). Stellar micro-variability becomes particularly important for present and future space missions such as MOST, COROT, KEPLER, SIM, and GAIA (Hatzes 2002; Green et al. 2003; Aigrain et al. 2004; Matthews et al. 2004). In this context, granulation-related micro-variability is usually considered as a noise source. It should be appreciated, however, that this “noise” also carries information about the statistics of convective flows. Whether considered as noise or signal: a better *theoretical characterization of granulation-related micro-*

variability would aid the planning and interpretation of upcoming observations.

Based on detailed radiation-hydrodynamics simulations of convective surface flows – similar to the ones described in Wedemeyer et al. (2004) – we want to predict the properties of granulation-related micro-variability in late-type stars. To our knowledge the work of Trampedach et al. (1998) is the only example of such a theoretical effort to date. Trampedach et al. studied the brightness and radial velocity variability in the Sun, α Cen A, and Procyon A. Their hydrodynamical models, as well as the ones we refer to, are so-called “local-box” models. They simulate convection in a small, representative volume located within the stellar surface layers. In order to derive observable, disk-integrated quantities, properties of the local model have to be extrapolated to the full stellar disk.

This paper outlines the statistical procedure that we employ for that purpose. It is intended as a precursor to later work presenting simulation results. While the statistical developments are mostly straightforward, we nevertheless feel that a somewhat detailed discussion is necessary to judge later results and – perhaps even more important – their inherent uncertainties. In the following we consider brightness fluctuations and fluc-

tuations in the position of the stellar photocenter. We do not consider the important case of fluctuations in spectroscopic radial velocity, basically since related spectral line formation issues complicate the problem. Despite its mostly technical nature, this paper contains some results within a broader scope so that the non-technically oriented reader might also find it of interest.

The paper is organized in the following way: in Sect. 2 we start by stating the basic statistical assumptions made when extrapolating from the local simulations to the full stellar disk, and describe in Sect. 3 what kind of simulation data did enter. In Sect. 4 we consider statistical properties of an individual simulation patch, and in Sect. 5 we continue by deriving the related formulae for the expectation value, variance, and power spectra of temporal brightness and positional variations of disk-integrated quantities. We show that there is a general close connection between brightness and positional variations, and that – a somewhat counter-intuitive result – photocentric variations do not depend on stellar radius but on the atmospheric parameters alone. Along the way, we introduce an approximation related to the well-known Eddington approximation to mitigate some numerical shortcomings. In Sect. 6 we add some cautionary comments about short-cuts when evaluating supposedly disk-integrated quantities from the flux data of a simulation box. In Sect. 7 we discuss an illustrative analytical model of brightness and positional variations, and make the connection between simulation patches and convective cells. In Sect. 8 we give our conclusions.

2. Basic statistical assumptions

Our goal was to make predictions of a star’s brightness fluctuations and of the displacements of its photocenter introduced by granulation, resorting to results of radiation-hydrodynamics simulations. These simulations provide a statistically representative, small, rectangular patch (or “tile”) of the emergent radiation field and its temporal evolution on the stellar surface. We imagined the visible stellar hemisphere as tiled by a possibly large number of simulation patches. Luckily, we did not have to construct this tiling, which would have been difficult in practice due to the periodic lateral boundary conditions employed in the simulations, among other problems. To derive what a distant observer would record if observing the unresolved stellar disk, we made the following statistical and physical assumptions:

- Each patch radiates statistically independent of all other patches.
- All patches on the stellar surface share the same statistical properties.
- The space-wise statistics of the patches on the stellar surface can be replaced by the time-wise statistics of a simulated patch.

In a real star the first assumption is not exactly fulfilled. In particular, acoustic modes have correlation lengths which introduce a coupling over scales larger than are typically encompassed by a simulation box. The coupling between modes and convection is too weak to introduce a mode-related long-range

correlation into the convective part of the flow, so that the first assumption should hold for granulation itself. The modal part could be treated separately as a perfectly correlated signal. In supergiants one might encounter limits to a statistical treatment of convection-related variability, since only very few granules cover the stellar surface (e.g., Freytag 2003). In appendix B we comment on testing the assumption of the statistical independence of a simulation patch. The second assumption expresses the notion of homogeneity. Again, in a real star, rotation or large-scale magnetic fields might lead to deviations from homogeneity. The last assumption is a statement about ergodicity, which appears justified considering the chaotic nature of stellar granular flows (Steffen & Freytag 1995). All in all, we feel that the above assumptions are not too critical in view of the precision we hope to achieve. Instead limitations of the simulations themselves – in particular the limited statistics due to the finite length of the calculated time series – control the accuracy of predictions at the moment.

3. The radiative output of a simulation patch

In the hydrodynamical simulations, the radiative energy exchange is treated in great detail: the geometry of the radiating flow is taken into account by a ray-tracing technique, and the wavelength dependence by a number of wavelength bands representing the effects of radiative heating or cooling in the continuum and spectral lines. While we concentrate in the following on wavelength integrated (“white light”) quantities, the formulas derived below also hold for variables which are measured at a particular wavelength, or which are integrals over a wavelength interval.

The basic radiative output that a simulation provides and that is relevant here, are surface averages of the emergent intensity I_m for various inclination cosines μ_m , $m \in \{1, \dots, M\}$; i.e. the detailed spatial intensity information of a simulation is reduced to a level familiar from 1D standard plane-parallel model atmospheres. However, the average intensities are computed for every time step, and are thus provided as a function of time $I_m(t)$.

The discrete set of inclinations and azimuthal angles is rather small reflecting limits imposed by the available computing resources. Typically, we worked with two or three angles in μ - and four in φ -direction. Table 1 summarizes the employed inclinations and associated weighting factors for evaluating the radiative flux. The integration scheme with, in total, three inclinations $M = 3$ is a Gauss-Lobatto type integration scheme (e.g., Abramowitz & Stegun 1972), while $M = 2$ is not. The $M = 2$ case is computationally quite economic for representing the center-to-limb behavior in the flux calculation but has some disadvantages when it comes to calculating the photocentric variability, as we discuss in detail later.

4. The statistics of the emergent flux of an individual simulation patch

In the following, we derive expressions both for the temporal average of the emergent flux of a simulation patch and for its standard deviation. Within the discretization of the radiative

Table 1. Inclination cosines μ_m and weighting factors w_m for the flux integration schemes with a total number of inclinations of $M = 2$ and $M = 3$. Factor $w_m\mu_m^2$ is given due to its importance for evaluating some disk-integrated quantities.

	$M = 2$		$M = 3$		
m	1	2	1	2	3
μ_m	1.0000	0.3333	1.0000	0.7651	0.2852
w_m	0.2500	0.7500	0.0667	0.3785	0.5549
$w_m\mu_m^2$	0.2500	0.0833	0.0667	0.2216	0.0451

transfer equation that is used in the hydrodynamical simulations, the horizontal average of the emergent flux F (more precisely of its vertical component) of a simulation patch is given by

$$F \equiv \oint d\Omega \mu I = \int_0^1 d\mu \int_0^{2\pi} d\varphi \mu I \simeq 2\pi \sum_{m=1}^M \sum_{k=1}^{\tilde{N}_m} w_{km} \mu_m I_{km} \quad (1)$$

where w_{km} is the fraction of the solid angle of the hemisphere at inclination μ_m and at azimuthal angle φ_k (see Fig. 1), and I_{km} the intensity in that direction. Here and in the following, the symbol “ \simeq ” denotes the approximate equality between continuous expressions and discrete analogs, where the induced errors vanish in the limit of infinitely fine discretization. We denote physical approximations by “ \approx ”. Statistically, the convection pattern is horizontally isotropic. Therefore, all weights belonging to the same μ -ring m (for the definition see Fig. 1) are made equal since the discretization in the azimuthal direction should reflect the isotropy. The weights differ between different μ -rings. Introducing the total weight w_m of the μ -ring m , the weights w_{km} are normalized so that

$$\sum_{m=1}^M \sum_{k=1}^{\tilde{N}_m} w_{km} = \sum_{m=1}^M \tilde{N}_m w_{km} = \sum_{m=1}^M w_m = 1 \quad (2)$$

where $\tilde{N}_m = w_m/w_{km}$ is the total number of solid angle elements belonging to the μ -ring m . For later reference, we give the discrete analog of the integral operator associated with the μ -integration

$$\int_0^1 d\mu g(\mu) \simeq \sum_{m=1}^M w_m g_m \quad (3)$$

where g is an arbitrary function of μ and $g_m = g(\mu_m)$. With (1) we obtain for the temporal average of the radiative flux F of a patch

$$\langle F \rangle \simeq 2\pi \sum_{m=1}^M \sum_{k=1}^{\tilde{N}_m} w_{km} \mu_m \langle I_{km} \rangle, \quad (4)$$

since w_{km} and μ_m are time-independent. Here and in the following, $\langle g \rangle$ denotes the temporal expectation value of a quantity g . Due to the horizontal isotropy, all elements of the solid angle belonging to the same μ -ring share the same statistics

$$\langle I_{km} \rangle = \langle I_m \rangle \quad \forall k, m \quad (5)$$

and

$$\sigma_{I_{km}} = \sigma_{I_m} \quad \forall k, m \quad (6)$$

where σ_g denotes the standard deviation of a variable g according to

$$\sigma_g \equiv \sqrt{\langle g^2 \rangle - \langle g \rangle^2}. \quad (7)$$

Using the isotropy, we finally obtain for the temporal average of the emergent flux

$$\langle F \rangle \simeq 2\pi \sum_{m=1}^M w_m \mu_m \langle I_m \rangle. \quad (8)$$

Now, we want to obtain an expression for the expectation value of F^2 introducing variances and correlation coefficients among the intensities going into different directions of the solid angle. The variances and correlation coefficients could be evaluated from the data provided by the hydrodynamical simulation. Of course, if one were interested in the flux variations of the simulation alone, one could resort to the flux directly evaluated from Eq. (1) and would not – rather indirectly – turn to the variances and correlation coefficients of the individual intensities. We derive the equations to compare them later with expressions for quantities integrated over the stellar disk. Using the basic relation (1) we obtain

$$\langle F^2 \rangle \simeq (2\pi)^2 \sum_{m=1}^M \sum_{m'=1}^M \sum_{k=1}^{\tilde{N}_m} \sum_{k'=1}^{\tilde{N}_{m'}} w_{km} w_{k'm'} \mu_m \mu_{m'} \langle I_{km} I_{k'm'} \rangle. \quad (9)$$

We introduce the linear correlation coefficient between I_{km} and $I_{k'm'}$, $C[I_{km}, I_{k'm'}]$, obeying the relation

$$\begin{aligned} \langle I_{km} I_{k'm'} \rangle &= \langle I_{km} \rangle \langle I_{k'm'} \rangle + \sigma_{I_{km}} \sigma_{I_{k'm'}} C[I_{km}, I_{k'm'}] \\ &= \langle I_m \rangle \langle I_{m'} \rangle + \sigma_{I_m} \sigma_{I_{m'}} C[I_{km}, I_{k'm'}] \end{aligned} \quad (10)$$

with which we can rewrite expression (9) as

$$\begin{aligned} \langle F^2 \rangle &\simeq (2\pi)^2 \sum_{m=1}^M \sum_{m'=1}^M \sum_{k=1}^{\tilde{N}_m} \sum_{k'=1}^{\tilde{N}_{m'}} \\ &w_{km} w_{k'm'} \mu_m \mu_{m'} \left(\langle I_m \rangle \langle I_{m'} \rangle + \sigma_{I_m} \sigma_{I_{m'}} C[I_{km}, I_{k'm'}] \right) \\ &= \langle F \rangle^2 + (2\pi)^2 \sum_{m=1}^M \sum_{m'=1}^M \sum_{k=1}^{\tilde{N}_m} \sum_{k'=1}^{\tilde{N}_{m'}} \\ &w_{km} w_{k'm'} \mu_m \mu_{m'} \sigma_{I_m} \sigma_{I_{m'}} C[I_{km}, I_{k'm'}]. \end{aligned} \quad (11)$$

To progress on the analytical side, we consider two limiting and one intermediate case for the behavior among the individual intensities emerging from a simulation patch:

i) The intensities of all elements of the solid angle are uncorrelated, i.e.,

$$C[I_{km}, I_{k'm'}] = \delta_{mm'} \delta_{kk'} \quad \forall m, m', k, k'. \quad (12)$$

ii) All intensities are perfectly positively correlated, i.e.,

$$C[I_{km}, I_{k'm'}] = 1 \quad \forall m, m', k, k'. \quad (13)$$

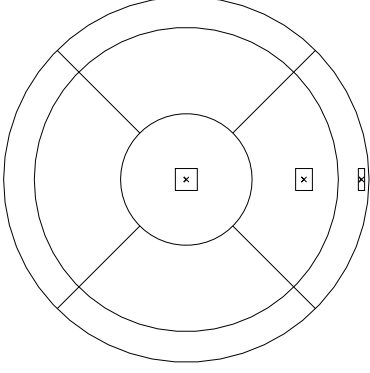


Fig. 1. Illustration of the weighting entering the calculation of the radiative flux. The plot shows the projection of a hemisphere, the concentric rings (in the text referred to as “ μ -rings”) and radial lines delineate the discrete elements of the solid angle (respective surface area elements for the integration over the stellar disk) entering the flux integration. Crosses mark the inclinations used for representing the angular dependence of the radiation field. The rectangles show how a square-shaped patch positioned on the surface at the various inclination angles appears foreshortened along the line of sight towards the limb. The diagram depicts the case $M = 3$ of Table 1.

iii) The intensities are correlated for all azimuthal angles belonging to the same inclination $\tilde{\mu}$, but are uncorrelated among different inclinations, i.e.,

$$C[I_{km}, I_{k'm'}] = \delta_{mm'} \quad \forall m, m', k, k'. \quad (14)$$

Case ii) often provides a good description of the actual behavior found for the intensities of an individual patch. Case iii) is also a plausible behavior, since different inclinations correspond to different heights in the atmosphere; one would expect that first the correlation between different height levels is lost before the azimuthal correlation is reduced. In the three cases we obtain for the variance of the flux of an individual patch

$$\sigma_F^2 \approx (2\pi)^2 \begin{cases} \sum_{m=1}^M \tilde{N}_m^{-1} w_m^2 \mu_m^2 \sigma_{I_m}^2 & \text{if } C[I_{km}, I_{k'm'}] = \delta_{mm'} \delta_{kk'} \\ \left(\sum_{m=1}^M w_m \mu_m \sigma_{I_m} \right)^2 & \text{if } C[I_{km}, I_{k'm'}] = 1 \\ \sum_{m=1}^M w_m^2 \mu_m^2 \sigma_{I_m}^2 & \text{if } C[I_{km}, I_{k'm'}] = \delta_{mm'}. \end{cases} \quad (15)$$

According to (11), σ_F is the sum of positive quantities so that as relation among the cases we find

$$\sigma_F^{(ii)} \geq \sigma_F^{(iii)} \geq \sigma_F^{(i)}, \quad (16)$$

reflecting the higher degree of cancellation for increasing degree of de-correlation.

5. Statistics of the disk-integrated, observable quantities

We now want to derive expressions for the brightness and positional fluctuations that a distant observer would record when observing the unresolved stellar disk.

5.1. General statistical relations

We are confronted with two problems: first, we have to introduce a correlation length on the surface of the sphere describing the two-point spatial correlation of the temporal granular intensity signal. This we have done – as outlined before – by considering the stellar surface as composed of identical patches which are statistically independent from one another but share similar statistical properties. We replace the gradual behavior of the correlation function by a step-like behavior which simplifies the treatment of the problem tremendously. Second, we have to make best contact to the data that the simulations provide. The central point is how we describe the center-to-limb variation. The basic idea is to transfer the discretization of the solid angle used in the hydrodynamical simulation to a corresponding partitioning of the stellar disk; i.e., we interpret the discretization of the solid angle from Table 1 as a partitioning of the visible stellar surface, as depicted in Fig. 1. This is of course analogous to the way the flux of a standard plane-parallel atmosphere model is translated to the disk integrated flux. Since we use a similar discretization of the stellar surface as in the case of integration over solid angle, the statistical formulae describing the flux of an individual simulation patch and disk-integrated emission will look almost identical. This is intentional. However, as will become apparent below, there are a number of subtleties which deserve some attention and may affect the final outcome substantially.

Algebraically, we proceed by starting with the continuous description of a quantity, and discretize into patches to introduce the finite correlation length. We then return to the continuous description, since the analytical manipulations are most easily done in this representation. To finally establish contact with the simulation data, we discretize again applying the scheme used in the hydrodynamical model.

We start by listing the discrete and continuous versions of the involved integral operators. Using the patches as discrete elements, the surface integral of a function $g(\mu = \cos \vartheta, \varphi)$ over the stellar hemisphere can be written as

$$\oint dA g(\mu, \vartheta) = \int_0^1 d\mu \int_0^{2\pi} d\varphi R^2 g(\mu, \vartheta) \approx \sum_{k=1}^N A g_k \quad (17)$$

where $g_k = g(\mu_k, \varphi_k)$, and μ_k and φ_k are the coordinates of patch k . The star’s radius is R , and N is the total number of patches on the curved surface of the visible stellar hemisphere; all patches have the same surface area $A = R^2 \Delta\mu \Delta\varphi$, so that

$$NA = 2\pi R^2. \quad (18)$$

For formal reasons we relate the surface tiling to a spherical coordinate system, but in fact do not envision the stellar surface tiled by segments suggested by such a system. The tiling should be considered as locally close to isotropic — as would be the case for the tiling of a plane by squares. We repeat that an explicit construction of a tiling turns out to be unnecessary.

We now formally define intensity-weighted integrals J_g of an arbitrary function g as

$$J_g \equiv \oint dA \mu I g. \quad (19)$$

This definition is introduced to streamline our nomenclature. We shall later set $g = 1$, and $g = x$ where x is the Cartesian x -position of a patch on the stellar disk. J_1 is related to the stellar flux, and J_x to the position of the stellar photocenter.

Similar to the angular integration we now make assumptions about the statistics of the patches. To preserve axisymmetric conditions, the temporal expectation of the intensity should be a function of μ alone

$$\langle I \rangle(\mu, \varphi) = \langle I \rangle(\mu). \quad (20)$$

Analogously, the standard deviation of the intensity should obey

$$\sigma_I(\mu, \varphi) = \sigma_I(\mu). \quad (21)$$

5.1.1. Temporal expectation value of J_g

In the following we consider a time-independent function $g(\mu, \varphi)$. With the previous assumptions about the μ -dependence of the intensity and its variance, we obtain for the temporal expectation value of J_g

$$\langle J_g \rangle = \int_0^1 d\mu \int_0^{2\pi} d\varphi R^2 \mu \langle I \rangle g = 2\pi R^2 \int_0^1 d\mu \mu \langle I \rangle g, \quad (22)$$

where the last equality holds if g is also φ -independent.

5.1.2. Temporal variance of J_g

The temporal expectation of J_g^2 depends on the properties of the spatial correlation of the intensity, similar to the flux of a simulation patch as expressed by Eq. (9). We now introduce the discretization into patches (17), which allows us to express these properties easily. The accuracy of this rests on the assumption that the patch size is small enough in comparison to the global stellar scale that position-dependent quantities (like the time-averaged intensity and g) vary little across the patch, but large enough that spatial correlations among statistical quantities across patches are negligible. We obtain

$$\begin{aligned} \langle J_g^2 \rangle &\simeq A^2 \sum_{k=1}^N \sum_{k'=1}^N \mu_k \mu_{k'} \langle I_k I_{k'} \rangle g_k g_{k'} \\ &= \langle J_g \rangle^2 + A^2 \sum_{k=1}^N \sum_{k'=1}^N \mu_k \mu_{k'} \sigma_{I_k} \sigma_{I_{k'}} g_k g_{k'} C[I_k, I_{k'}], \end{aligned} \quad (23)$$

where the intensity I_k is the surface average over patch k in the direction towards the observer. In the present context summation index k does not refer to a particular coordinate direction but merely numbers the patches located on the stellar surface. This reflects the fact that we discuss correlations among the intensities emitted by different patches and not within one patch as considered in Sect. 4. The discretization into patches is not related to the partitioning of the stellar disk as depicted in Fig. 1. This is introduced at a later stage. We are mostly interested in the case where the individual patches are statistically independent, i.e., $C[I_k, I_{k'}] = \delta_{kk'}$. However, to enable comparison with the formulae derived for the flux of an individual

patch, we also consider the case of perfect positive correlation, i.e., $C[I_k, I_{k'}] = 1$. For the case of statistical independence, we obtain

$$\sigma_{J_g}^2 \simeq A^2 \sum_{k=1}^N \mu_k^2 \sigma_{I_k}^2 g_k^2 \simeq AR^2 \int_0^1 d\mu \int_0^{2\pi} d\varphi \mu^2 \sigma_I^2 g^2. \quad (24)$$

Note, that relation (24) becomes asymptotically exact if the spatial correlation length of σ_I^2 goes to zero. For a φ -independent g , we get

$$\begin{aligned} \sigma_{J_g}^2 &= 2\pi R^2 A \int_0^1 d\mu \mu^2 \sigma_I^2 g^2 = (2\pi)^2 R^4 N^{-1} \int_0^1 d\mu \mu^2 \sigma_I^2 g^2 \\ &\simeq (2\pi)^2 R^4 N^{-1} \sum_{m=1}^M w_m \mu_m^2 \sigma_{I_m}^2 g_m^2 \end{aligned} \quad (25)$$

where in the last equality we introduced the segmentation (3).

For the second case of a coherent behavior of the patches, again specializing for the case of a φ -independent g , we obtain

$$\sigma_{J_g}^2 = \left(2\pi R^2 \int_0^1 d\mu \mu \sigma_I g \right)^2 \simeq (2\pi)^2 R^4 \left(\sum_{m=1}^M w_m \mu_m \sigma_{I_m} g_m \right)^2. \quad (26)$$

In summary, for $g(\mu, \varphi) = g(\mu)$ in the two cases we obtained

$$\sigma_{J_g}^2 = (2\pi)^2 R^4 \begin{cases} N^{-1} \int_0^1 d\mu \mu^2 \sigma_I^2 g^2 & \text{if } C[I_k, I_{k'}] = \delta_{kk'} \\ \left(\int_0^1 d\mu \mu \sigma_I g \right)^2 & \text{if } C[I_k, I_{k'}] = 1, \end{cases} \quad (27)$$

or the discrete analog using (3)

$$\sigma_{J_g}^2 \simeq (2\pi)^2 R^4 \begin{cases} N^{-1} \sum_{m=1}^M w_m \mu_m^2 \sigma_{I_m}^2 g_m^2 & \text{if } C[I_k, I_{k'}] = \delta_{kk'} \\ \left(\sum_{m=1}^M w_m \mu_m \sigma_{I_m} g_m \right)^2 & \text{if } C[I_k, I_{k'}] = 1. \end{cases} \quad (28)$$

At this point we would also like to emphasize a general feature of the formulae derived here and in the following: one might (erroneously) conclude from formula (28) that $\sigma_{J_g}^2$ depends on the particular, and to some extent arbitrary, geometry of the simulation patch since N and σ_{I_m} depend on the patch size. However, only their combination σ_{I_m} / \sqrt{N} enters the relations. This combination is invariant to changes in the patch geometry, as long as our basic assumption holds that a patch represents a statistically independent surface element. Hence, $\sigma_{J_g}^2$ is in fact independent of the particular patch geometry.

5.1.3. Temporal power spectrum of J_g

To characterize the statistics of J_g further by its temporal power spectrum, we only consider the case of statistically independent patches. In the following, $\hat{y}(\omega)$ denotes the temporal Fourier component of a time-dependent variable $y(t)$, and \hat{y}^* the conjugate complex. Taking the Fourier transform of both sides of the basic definition (19), we get for an Fourier component of J_g

$$\hat{J}_g = \oint dA \mu \hat{I} \simeq \sum_{k=1}^N A \mu_k \hat{I}_k g_k \quad (29)$$

where we assumed that g is time-independent. Accordingly, for a frequency component of the power spectrum we obtain

$$\hat{J}_g \hat{J}_g^* \simeq \sum_{k=1}^N \sum_{k'=1}^N A^2 \mu_k \mu_{k'} \hat{I}_k \hat{I}_{k'}^* g_k g_{k'}. \quad (30)$$

This expresses the power of a frequency component for a particular realization of a convection pattern and its evolution. We now have to average over all possible realizations to estimate the expectation value of the power. Denoting the ensemble average as $\langle g \rangle_{\text{ens}}$, we obtain

$$\langle \hat{J}_g \hat{J}_g^* \rangle_{\text{ens}} \simeq \sum_{k=1}^N \sum_{k'=1}^N A^2 \mu_k \mu_{k'} \langle \hat{I}_k \hat{I}_{k'}^* \rangle_{\text{ens}} g_k g_{k'}. \quad (31)$$

All realizations share the property that the amplitude of a particular Fourier component \hat{I}_k is the same. Among the realizations, the \hat{I}_k -components only differ by a uniformly distributed random phase factor $\exp(i\phi_{kk'})$. The difference between two uniformly distributed random phases is again a uniformly distributed random phase. It follows that

$$\langle \hat{I}_k \hat{I}_{k'}^* \rangle_{\text{ens}} = |\hat{I}_k| |\hat{I}_{k'}^*| \langle e^{i\Delta\phi_{kk'}} \rangle_{\text{ens}} = \hat{I}_k \hat{I}_{k'}^* \delta_{kk'}. \quad (32)$$

The last equality comes about because for $k \neq k'$ the ensemble average $\langle e^{i\Delta\phi_{kk'}} \rangle_{\text{ens}}$ corresponds to an average over the unit circle in the complex plane which is zero. For $k = k'$ the phase difference is not random but always zero, and the ensemble average is one. From now on we drop the subscript “ens” indicating the ensemble average, but keep in mind that with respect to average power, angular brackets denote ensemble averages. One should further keep in mind that the hydrodynamical models provide only an estimate of the average power of the intensity $\hat{I}_k \hat{I}_k^*$, because only a finite time interval is simulated.

With the formula for the ensemble average of the power of the intensity we obtain for the power of J_g

$$\begin{aligned} \langle \hat{J}_g \hat{J}_g^* \rangle &\simeq \sum_{k=1}^N A^2 \mu_k^2 \langle \hat{I}_k \hat{I}_k^* \rangle g_k^2 \\ &\simeq AR^2 \int_0^1 d\mu \int_0^{2\pi} d\varphi \mu^2 \langle \hat{I} \hat{I}^* \rangle g^2. \end{aligned} \quad (33)$$

Similar to Eq. (24) the above relation becomes asymptotically exact, if the spatial correlation length of the intensity goes to zero. Assuming a φ -independent g , we finally obtain

$$\begin{aligned} \langle \hat{J}_g \hat{J}_g^* \rangle &= (2\pi)^2 R^4 N^{-1} \int_0^1 d\mu \mu^2 \langle \hat{I} \hat{I}^* \rangle g^2 \\ &\simeq (2\pi)^2 R^4 N^{-1} \sum_{m=1}^M w_m \mu_m^2 \langle \hat{I}_m \hat{I}_m^* \rangle g_m^2. \end{aligned} \quad (34)$$

Note, that the above relation for the expectation value of a frequency component of the power spectrum of J_g is consistent with the relation for its variance (28): the frequency integral of the power (excluding zero frequency) equals the variance of the signal as expressed by Parseval’s theorem.

5.2. Statistics of the observable flux

We now apply the previously derived formulae to evaluate statistical properties of the observable flux. The flux f observed at a distance D from the star is related to the moment J_1 according to $J_1 = D^2 f$. Due to this close connection we shall sometimes loosely refer to J_1 as observable flux.

5.2.1. The expectation value of the observable flux

From Eq. (22) setting $g = 1$ and the basic definition of the flux of an individual patch (1), we obtain for a φ -independent mean intensity $\langle I_m \rangle$

$$\langle J_1 \rangle = 2\pi R^2 \int_0^1 d\mu \mu \langle I \rangle = R^2 \langle F \rangle, \quad (35)$$

or

$$\langle f \rangle = \frac{R^2}{D^2} \langle F \rangle. \quad (36)$$

The observed temporally averaged flux – perhaps no surprise – is the average flux of an individual patch reduced by the distance-related factor R^2/D^2 . At this point one might be tempted to ignore the fact that Eq. (36) expresses a relation between the expectation values of f and F , not the fluxes themselves, and might calculate a power spectrum of the disk-integrated flux as a power spectrum of the flux of the simulation patch, perhaps scaled by the factor N^{-1} . We discuss the quantitative error of this approximate procedure in Sect. 6.

5.2.2. The variance of the observable flux

To compute the variance of the observable brightness fluctuations, we need to obtain the second moment of J_1 . As in the case of an individual simulation patch, we consider the two limiting cases of statistical independence and perfect positive correlation. Applying Eq. (28) results in

$$\begin{aligned} \sigma_f^2 &= \frac{\sigma_{J_1}^2}{D^4} \\ &\simeq (2\pi)^2 \left(\frac{R}{D} \right)^4 \begin{cases} N^{-1} \sum_{m=1}^M w_m \mu_m^2 \sigma_{I_m}^2 & \text{if } C[I_k, I_{k'}] = \delta_{kk'} \\ \left(\sum_{m=1}^M w_m \mu_m \sigma_{I_m} \right)^2 & \text{if } C[I_k, I_{k'}] = 1. \end{cases} \end{aligned} \quad (37)$$

We find – perhaps again no surprise – that in the case of statistical independence the variance of the observable flux scales inversely proportional to the number of patches on the visible stellar surface. Relations (37) are close to the results for an individual patch (15). We can make it even closer by introducing the number of patches N_m located within μ -ring m of the stellar disk

$$N_m = w_m N, \quad (38)$$

since all patches on the stellar surface have the same area.

Since the weights in the solid angle integration are not proportional to the number of solid angle elements, Eq. (15) cannot, on the other hand, be cast in the form of Eq. (37). Introducing (38) makes Eq. (37) read

$$\sigma_f^2 \simeq (2\pi)^2 \left(\frac{R}{D} \right)^4 \begin{cases} \sum_{m=1}^M N_m^{-1} w_m^2 \mu_m^2 \sigma_{I_m}^2 & \text{if } C[I_k, I_{k'}] = \delta_{kk'} \\ \left(\sum_{m=1}^M w_m \mu_m \sigma_{I_m} \right)^2 & \text{if } C[I_k, I_{k'}] = 1. \end{cases} \quad (39)$$

Only in the (for convective flows) unrealistic situation of a perfect correlation among the intensities of a patch and also among the intensities across the stellar disk, one can directly relate disk-integrated brightness fluctuations to the fluctuations of the flux of the patch as $\sigma_{J_1} = R^2 \sigma_F$ which is analogous to the relation for the flux $\langle J_1 \rangle = R^2 \langle F \rangle$. In all other cases one has to

resort to the intensities themselves. Even if one chose to make all elements of the angular integration the same size, and obtained a direct correspondence of the formulae this way, one still could not use the flux of the patch to derive the brightness fluctuation of the star as a whole. The reason is found in the different degrees of correlation among the intensities of a patch and across the disk. Within a patch the intensities going in various directions usually show a substantial degree of correlation, which is lacking for the intensities emerging from different locations on the stellar disk. We discuss this aspect quantitatively in Sect. 6.

5.2.3. Temporal power spectrum of the observable flux

To further characterize the statistics of the observable flux, we use Eq. (34) to write down its temporal power spectrum for the case of statistically independent patches

$$\langle \hat{J}_1 \hat{J}_1^* \rangle \simeq (2\pi)^2 R^4 N^{-1} \sum_{m=1}^M w_m \mu_m^2 \langle \hat{I}_m \hat{I}_m^* \rangle. \quad (40)$$

For the power spectrum of the observable, relative flux variations we obtain

$$\frac{\langle \hat{f} \hat{f}^* \rangle}{\langle f \rangle^2} = \frac{\langle \hat{J}_1 \hat{J}_1^* \rangle}{\langle J_1 \rangle^2} \simeq N^{-1} \frac{\sum_{m=1}^M w_m \mu_m^2 \langle \hat{I}_m \hat{I}_m^* \rangle}{\left(\sum_{m=1}^M w_m \mu_m \langle I_m \rangle \right)^2}. \quad (41)$$

We remind the reader that the angular brackets around frequency components of power spectra denote ensemble averages.

5.3. Statistics of the photocentric position

We consider the position of the stellar photocenter in Cartesian coordinates (x, y) . The origin of the Cartesian coordinate system is placed in the geometrical center of the stellar disk. We again assume statistically isotropic conditions with respect to disk center. x - and y -direction are equivalent, and we only have to regard – without loss of generality – one Cartesian coordinate, say x . The position of the photocenter $x_{\text{ph}}(t)$ is given as the intensity-weighted mean of the x -positions of all light emitting patches tiling the visible stellar surface according to

$$x_{\text{ph}} \equiv \frac{J_x}{J_1} = \frac{J_x}{\langle J_1 \rangle} \left[1 + \mathcal{O} \left(\frac{\sigma_{J_1}}{\langle J_1 \rangle} \right) \right]. \quad (42)$$

Since the relative fluctuations of the observable flux are small, we neglect the higher order terms in the fluctuations of J_1 and work with the second equality in Eq. (42). This leaves us with a much more convenient *linear* relationship between x_{ph} and the intensities. For obtaining the expectation value and variance of x_{ph} we now have to evaluate the respective quantities of J_x . We do this only for the case of uncorrelated patches, since it is clear that one would not obtain any motion of photocenter for the case of a perfectly correlated action of all patches.

To apply the previously derived formulae, we set $g = x$, in spherical coordinates

$$x = R \sqrt{1 - \mu^2} \cos \varphi. \quad (43)$$

5.3.1. Expectation value of the photocentric position

From Eq. (22) one immediately gets

$$\langle J_x \rangle = \int_0^1 d\mu \int_0^{2\pi} d\varphi R^3 \mu \langle I \rangle \sqrt{1 - \mu^2} \cos \varphi = 0, \quad (44)$$

and

$$\langle x_{\text{ph}} \rangle = 0, \quad (45)$$

since the φ -integral vanishes. The expectation value of the photocenter's position coincides with the geometric center of the star. This is of course a consequence of the fact that we – in a statistical sense – preserved axisymmetry in the formulation of the problem.

5.3.2. The variance of the photocentric position

To obtain the variance of the photocentric position, we have to evaluate $\langle J_x^2 \rangle$. From relation (24), valid for φ -dependent quantities, we get

$$\begin{aligned} \sigma_{J_x}^2 &= AR^4 \int_0^1 d\mu \int_0^{2\pi} d\varphi \mu^2 \sigma_I^2 (1 - \mu^2) \cos^2 \varphi \\ &= \frac{1}{2} R^2 \sigma_{J_1}^2 \left[1 - \frac{\int_0^1 d\mu \mu^4 \sigma_I^2}{\int_0^1 d\mu \mu^2 \sigma_I^2} \right], \end{aligned} \quad (46)$$

where we used the relation (see Eq. [25])

$$\sigma_{J_1}^2 = (2\pi)^2 R^4 N^{-1} \int_0^1 d\mu \mu^2 \sigma_I^2. \quad (47)$$

Equation (46) describes a relation between J_x and J_1 . We shall see later that the connection is even tighter than it might at first appear from Eq. (46), since it turns out that the term in angular brackets is only weakly variable with the degree of limb-darkening of σ_I^2 . Now we can write the variance of x_{ph} :

$$\sigma_{x_{\text{ph}}}^2 = \frac{\sigma_{J_x}^2}{\langle J_1 \rangle^2} = \frac{A}{4\pi} \frac{\int_0^1 d\mu \mu^2 \sigma_I^2}{\left(\int_0^1 d\mu \mu \langle I \rangle \right)^2} \left[1 - \frac{\int_0^1 d\mu \mu^4 \sigma_I^2}{\int_0^1 d\mu \mu^2 \sigma_I^2} \right]. \quad (48)$$

Remarkably, the variance of the photocentric position is independent of stellar radius (or equivalently total number of patches), as long as we assume that the patch size A and its radiation properties are fixed. Astrophysically, this means that a star's photocentric variability¹ depends only on its atmospheric parameters (T_{eff} , $\log g$, and chemical composition). However, when changing a star's radius at fixed surface conditions by altering its mass, the relative importance of sphericity is changed. This is a higher order effect but might bring a radius dependence back in for objects with extended atmospheres. The radius independence is intrinsic to the particular 2D axisymmetric geometry of the problem. It can be shown that the same does not hold, e.g., for a linear chain of patches. From a practical point of view it is convenient that we do not have to

¹ Note that we are discussing the absolute spatial variability of the photocenter, hence the stellar distance does not enter at this point.

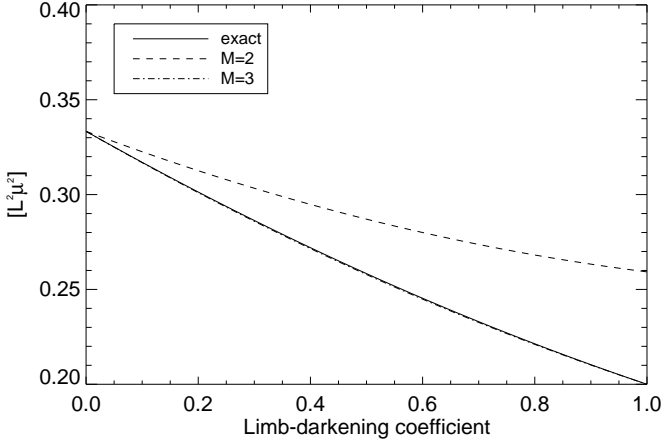


Fig. 2. Comparison of the integral $\int_0^1 d\mu L^2 \mu^2$, which enters the evaluation of $\sigma_{J_1}^2$ (see Eq. [47]). For a typical limb-darkening around $a = 0.6$, we obtain a difference of 13 % to the exact result in the case $M = 2$. In the case $M = 3$, differences are negligible.

specify a precise stellar radius when evaluating the variance of the displacement of the photocenter.

We have not written down the discrete analogs of Eqs. (46) and (48) yet, because a numerical problem exists when evaluating integrals involving higher powers of μ . The integrals become inaccurate; this is particularly the case for our integration scheme with $M = 2$, which is not a Gauss-Lobatto type integration. We now seek a way to mitigate the problem. To illustrate the situation, we assume that the dependence of the expectation value of the intensity on μ follows a linear limb-darkening law L of the form

$$\frac{\langle I \rangle(\mu)}{\langle I \rangle(\mu = 1)} = L(\mu) = 1 - a + a\mu \quad (49)$$

where a is the limb-darkening coefficient. The numerical results of the hydrodynamical simulation show that the standard deviation of the intensity is often roughly proportional to the intensity. Hence, it is reasonable to assume a similar behavior for the standard deviation

$$\frac{\sigma_I(\mu)}{\sigma_I(\mu = 1)} = L(\mu). \quad (50)$$

Using the linear limb-darkening laws (49) and (50), the integrals in Eq. (48) can be evaluated analytically (see appendix A), as well as numerically. The results can be compared to estimate the error introduced by the various integration schemes.

Figure 2 shows the comparison between the exact and numerical results for the integral $\int_0^1 d\mu L^2 \mu^2$, which enters the calculation of $\sigma_{J_1}^2$ (Eq. [47]). For a typical limb-darkening at optical wavelength we find a sizeable but tolerable integration error in the case $M = 2$. Case $M = 3$ gives almost exact results. Consequently, we do not expect that the limited accuracy of our integration schemes will affect the evaluation of the photometric variability substantially.

As shown in Fig. 3, the situation deteriorates when considering the ratio $\int_0^1 d\mu L^2 \mu^4 / \int_0^1 d\mu L^2 \mu^2$, which enters the eval-

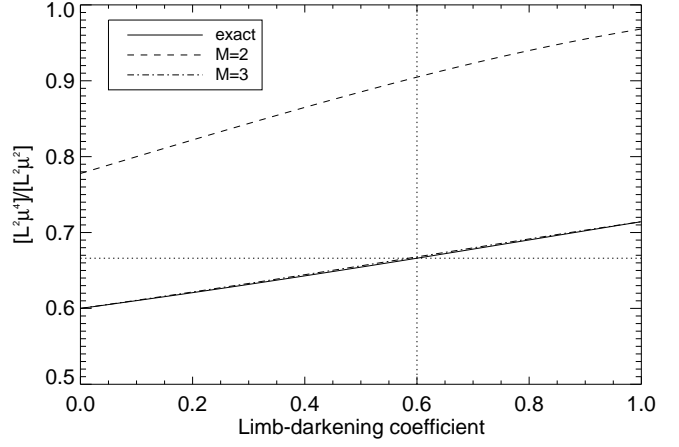


Fig. 3. Comparison of $\int_0^1 d\mu L^2 \mu^4 / \int_0^1 d\mu L^2 \mu^2$ which enters the computation of the displacement of the photocenter (see Eq. [48]). For a typical limb-darkening around $a = 0.6$, we obtain a difference of 30 % to the exact result in the $M = 2$ case. In the $M = 3$ case, differences are negligible.

uation of the displacement of the photocenter (Eq. [48]). However, the figure also shows that the exactly evaluated overall variation of the ratio of the two integrals is not large. In view of the large error associated with the numerical integration in the case $M = 2$, this leads to the idea of replacing the ratio of the integrals by a constant, representative value of the exact integral. We choose for the ratio

$$\frac{\int_0^1 d\mu L^2 \mu^4}{\int_0^1 d\mu L^2 \mu^2} \approx \frac{2}{3}, \quad (51)$$

which results from a limb-darkening coefficient of about $a = 0.6$. Apart from $a = 0.6$ being a reasonable value for the limb-darkening coefficient in the optical, a ratio of $\frac{2}{3}$ is chosen as a reminder that the approximation (51) is of course closely related to the well-known Eddington approximation, where a value of $\frac{1}{3}$ is assumed for the ratio between the second and zeroth angular moment of the intensity. For this reason we shall refer to approximation (51) as the *Eddington-like approximation*.

We apply the Eddington-like approximation to relations for the displacement of the photocenter (46) and (48). In doing so we hope to mitigate the effects of decreased numerical accuracy when evaluating the ratio $\int_0^1 d\mu L^2 \mu^4 / \int_0^1 d\mu L^2 \mu^2$. For the standard deviation σ_{J_x} , we obtain

$$\sigma_{J_x} \approx \frac{R}{\sqrt{6}} \sigma_{J_1}, \quad (52)$$

or for the standard deviation of the photocenter $\sigma_{x_{\text{ph}}}$ itself,

$$\sigma_{x_{\text{ph}}} \approx \frac{R}{\sqrt{6}} \frac{\sigma_{J_1}}{\langle J_1 \rangle} = \frac{R}{\sqrt{6}} \frac{\sigma_f}{\langle f \rangle}. \quad (53)$$

Equation (53) relates the observable flux variations to the displacement of the photocenter. Remarkably, no information intrinsic to granulation enters this relation. Hence, the relation

could be more generally valid than the particular derivation might suggest. And indeed, e.g., Lindegren (1977) has derived a similar connection in the context of the astrometry of objects with an apparently time-variable surface pattern due to rotation. Equation (53) is a relation among quantities which should be directly accessible to observation. This might be considered an advantage. However, concerning convection as such, the diagnostic power of Eq. (53) is limited since the observed variations in brightness and position cannot be immediately connected to convection. Other processes can produce a similar signal.

Since the temporal power spectrum of the brightness fluctuations is closely linked to its variance, Eq. (53) also states that the power spectrum of the photocentric displacement is – up to the frequency independent factor $R^2/6$ – identical to the power spectrum of the relative brightness fluctuations. This is a very convenient property. The similarity between the power spectra of brightness and positional fluctuations does not imply a temporal correlation among these variables. In fact, one can immediately show that $C[J_1, J_x] = 0$ or, correspondingly, that the observable flux and the displacement of the photocenter are uncorrelated:

$$C[f, x_{\text{ph}}] = 0. \quad (54)$$

Hatzes (2002) discusses simultaneous measurements of correlated observables to improve signal-to-noise ratios in exoplanet searches. The observables discussed here do not offer such a possibility.

Using the Eddington-like approximation in Eq. (48), we alternatively obtain

$$\sigma_{x_{\text{ph}}} \approx \frac{l}{\sqrt{12\pi}} \frac{\left(\int_0^1 d\mu \mu^2 \sigma_I^2\right)^{\frac{1}{2}}}{\int_0^1 d\mu \mu \langle I \rangle} \approx \frac{l}{\sqrt{12\pi}} \frac{\left(\sum_{m=1}^M w_m \mu_m^2 \sigma_{I_m}^2\right)^{\frac{1}{2}}}{\sum_{m=1}^M w_m \mu_m \langle I_m \rangle}, \quad (55)$$

where we have introduced the linear patch size $l \equiv \sqrt{A}$. Again, formula (55) is manifestly radius-independent. It also gives the discrete expression for evaluating the standard deviation of the photocentric displacement.

6. Estimating σ_f from σ_F ?

In this section we briefly digress to discuss the relation between the flux variations of a simulation patch as given by Eq. (15), and the disk-integrated flux variations given by Eq. (37) more quantitatively. The reason is that one might take the standard deviation of the flux of a simulation patch scaled by $1/\sqrt{N}$ as a proxy for the standard deviation of the observable flux. One might proceed in the same way when calculating power spectra of the disk-integrated flux variations. For deriving an estimate of the introduced errors, we once again assume the linear limb-darkening laws (49) and (50). We evaluate the ratio of the relative standard deviations scaled by the total number of patches $\sqrt{N}(\sigma_f/f)/(\sigma_F/F)$. We consider the cases ii) and iii) (see Eq. [15]) of the angular correlation of the intensities of a patch, and compare those with the (realistic) case of a statistically independent behavior of the patches across the stellar surface. We restrict ourselves to cases ii) and iii), because they

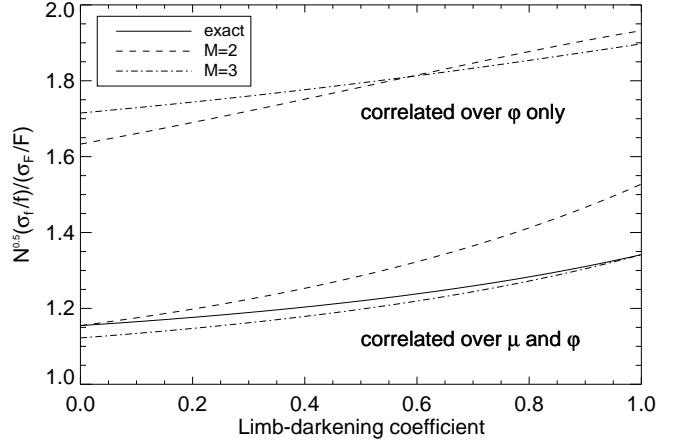


Fig. 4. The disk-to-patch ratio of relative flux variations as a function of the limb-darkening coefficient for two different assumptions about the angular correlation of the intensity within a patch.

encompass the actual range found for the angular intensity correlations within a patch. Figure 4 depicts the result. The exact result, i.e., analytically integrated angular integrals, is left out in the case of partial correlation, since no continuous analog of the discrete formula (15) (case iii) can be easily written down. It is of minor importance since what is relevant here are not the deviations from the exact result, but the absolute value of the disk-to-patch ratios.

Figure 4 shows that one tends to *underestimate* the amplitude of the observable brightness fluctuations, if one computes the fluctuations directly from the flux of a simulation patch and simply scales it by $1/\sqrt{N}$. Depending on the angular correlation of the intensities of the simulation patch, the error can become substantial. In the (not shown) case of completely uncorrelated intensities of a simulation patch, the error becomes even larger (a ratio of about 2 for $M = 2$, about 3.3 for $M = 3$, both for four azimuthal angles) than in the cases depicted in Fig. 4. The two reasons for the discrepancies have already been discussed in connection with Eqs. (37) and (39).

7. An analytical model for the case of a linear limb-darkening law

It is instructive to evaluate the formulae derived in Sects. 5.2 and 5.3 for the linear limb-darkening laws for I and σ_I (Eqs. (49) and [50]). From Eqs. (22), (28), and auxiliary formulae from appendix A, we directly obtain for the relative fluctuations in the observable flux for the case of uncorrelated patches

$$\frac{\sigma_f}{\langle f \rangle} = N^{-\frac{1}{2}} \frac{\sigma_I}{\langle I \rangle} \frac{\left(\int_0^1 d\mu L^2 \mu^2\right)^{\frac{1}{2}}}{\int_0^1 d\mu L \mu} = N^{-\frac{1}{2}} \frac{\sigma_I}{\langle I \rangle} \frac{\sqrt{\frac{1}{3} - \frac{a}{6} + \frac{a^2}{30}}}{\frac{1}{2} - \frac{a}{6}}. \quad (56)$$

Here $\langle I \rangle$ and σ_I should be understood as the values at $\mu = 1$. The a -dependent numerical factor in Eq. (56) has already been depicted in Fig. 4: the solid curve depicting the exact integral

in the case of complete correlation. Dependence on the limb-darkening coefficient a is only mild, but it shows that the brightness variations grow for a more pronounced limb-darkening.

Similarly, we obtain from Eq. (48) for the standard deviation of the photocentric displacement

$$\begin{aligned}\sigma_{x_{\text{ph}}} &= \frac{l}{\sqrt{4\pi}} \frac{\sigma_I}{\langle I \rangle} \frac{\left(\int_0^1 d\mu L^2 \mu^2 (1 - \mu^2) \right)^{\frac{1}{2}}}{\int_0^1 d\mu L \mu} \\ &= \frac{l}{\sqrt{4\pi}} \frac{\sigma_I}{\langle I \rangle} \frac{\sqrt{\frac{2}{15} - \frac{a}{10} + \frac{a^2}{42}}}{\frac{1}{2} - \frac{a}{6}}\end{aligned}\quad (57)$$

The a -dependent factor in Eq. (57) is only very weakly variable, as it varies (non-monotonically) between 0.201 and 0.206 with the limb-darkening coefficient in the interval $a \in [0, 1]$ so that to good approximation

$$\sigma_{x_{\text{ph}}} \approx 0.2 l \frac{\sigma_I}{\langle I \rangle}.\quad (58)$$

Formula (58) clearly emphasizes that the photocentric displacement does not depend on the stellar radius but only on local, granulation-related properties.

The chosen box-geometry of the hydrodynamical simulations sets the linear patch size, and the patch-averaged temporal intensity fluctuations scale with the surface area of the box. The natural statistically independent elements on the stellar surface are not patches but the granules, so that in physical terms one would like to connect l to the linear size of a granule and $\sigma_I / \langle I \rangle$ to the time-wise fluctuations of its emitted light. In the spirit of our basic assumption of ergodicity, we might further replace the time-wise fluctuations by equivalent space-wise fluctuations. We preliminarily find an approximate, empirical relation

$$l \frac{\sigma_I}{\langle I \rangle} \approx 0.4 l_{\text{gran}} \frac{\delta I_{\text{rms}}}{\bar{I}},\quad (59)$$

which, combined with Eq. (58), gives

$$\sigma_{x_{\text{ph}}} \approx 0.08 l_{\text{gran}} \frac{\delta I_{\text{rms}}}{\bar{I}}.\quad (60)$$

Here l_{gran} is the linear granular size – defined via the maximum in the spatial power spectrum of the intensity pattern – \bar{I} the spatial average of the intensity, and δI_{rms} the spatial root-mean-squares intensity contrast – (conventionally) defined at ideally infinite resolution, here the resolution of the computational grid. Equation (59) approximately relates the patch-connected quantities in Eq. (58) to physical properties of individual granules and the granulation pattern. Perhaps surprising at first glance, the numerical factor in Eq. (59) is not one but smaller than one, despite the fact that the product $l \sigma_I / \langle I \rangle$ should be scale-invariant, as long as no spatial correlations are present on the considered scales. The intensity contrast in Eq. (59) refers to scales smaller than the granular scale where this assumption is violated. On these scales the intensities are spatially correlated leading to enhanced fluctuations relative to

larger scales, which needs to be compensated for by a numerical factor smaller than one. Moreover, we also expect deviations from one due to the differences in geometry between square-shaped boxes and roundish granules.

As a rough estimate for the Sun from Eq. (60) with $l_{\text{gran}} \approx 1000$ km and $\delta I_{\text{rms}} / \bar{I} \approx 0.18$, we obtain a granulation induced photocentric variability of $\sigma_{x_{\text{ph}}} \approx 14$ km, $\approx 10^{-7}$ AU, or $\approx 0.1 \mu\text{s} / D$ [pc]. This already indicates that granulation will hardly affect the astrometry of dwarf stars at the precision level that is expected to be reached by the GAIA mission. The size of granules grows roughly inversely proportional to the surface gravity (Freitag et al. 1997) of a star, so that in giants and supergiants we expect much greater effects.

8. Conclusions and outlook

We derived formulae for evaluating the disk-integrated fluctuations of a star's brightness and the position of its photocenter from local-box hydrodynamical atmosphere models. Besides the merely technical results, we showed that there is a close connection between stellar photometric and photocentric variability. While derived here for granular surface patterns, the relation should be similar for any statistically homogeneous time-variable surface pattern. Activity related brightness patterns are an interesting case. Unfortunately, active regions are not expected to be homogeneously distributed over the stellar surface but to follow belt-like zones. We nevertheless expect that a semi-quantitative connection will still remain between activity-induced photometric and photocentric variability so that order-of-magnitude estimates of the photocentric variability are possible from measured brightness fluctuations. This may help in estimating limitations to the achievable astrometric accuracy for missions like GAIA. As we indicated in the previous section, effects due to granulation themselves are not likely to be important with the exception of extreme giants. This will be quantified in more detail in a subsequent paper. A preview of the simulation results can be found in Svensson & Ludwig (2005).

Acknowledgements. We would like to thank Lennart Lindegren and Matthias Steffen for their help concerning the algebra, statistical problems, and the presentation of the results. This work benefitted from financial support by the Swedish Research Council and the Royal Physiographic Society in Lund.

Appendix A: Angular integrals of $L^n \mu^m$

For a linear limb-darkening law of the form

$$L(\mu) = 1 - a + a\mu,\quad (A.1)$$

we find the following integrals over μ :

$$\int_0^1 d\mu L \mu = \frac{1}{2} - \frac{a}{6}\quad (A.2)$$

$$\int_0^1 d\mu L^2 \mu^2 = \frac{1}{3} - \frac{a}{6} + \frac{a^2}{30}\quad (A.3)$$

$$\int_0^1 d\mu L^2 \mu^4 = \frac{1}{5} - \frac{a}{15} + \frac{a^2}{105}\quad (A.4)$$

$$\int_0^1 d\mu L^2 \mu^2 (1 - \mu^2) = \frac{2}{15} - \frac{a}{10} + \frac{a^2}{42}.\quad (A.5)$$

Appendix B: Statistical independence of a patch and the spatial autocorrelation of the granulation pattern

One of our basic assumption is that the radiative output of a simulated patch can be regarded as statistically independent of all other patches. We might check this assumption by testing whether the assumption is already fulfilled within a simulation patch, i.e., whether parts of the patch are already distant enough to radiate independently. For this we have to evaluate the time-wise correlation coefficient of the emitted intensity at two locations (x, y) and (x', y') given by

$$C[I(x, y), I(x', y')] = \frac{\langle I(x, y)I(x', y') \rangle - \langle I(x, y) \rangle \langle I(x', y') \rangle}{\sigma_{I(x, y)} \sigma_{I(x', y')}} = \langle g(x, y)g(x', y') \rangle, \quad (\text{B.1})$$

where we introduced the normalized intensity

$$g \equiv \frac{I - \langle I \rangle}{\sigma_I}. \quad (\text{B.2})$$

Due to the horizontal statistical homogeneity of the granulation pattern, the correlation is expected not to depend on the absolute position but only on the distance between two points. To get an overall measure of the statistical dependence C among the various locations, one can spatially average over all pairs of points located a distance $(\Delta x, \Delta y)$ apart:

$$C(\Delta x, \Delta y) = \frac{1}{(x_2 - x_1)(y_2 - y_1)} \left\langle \int_{x_1}^{x_2} dx \int_{y_1}^{y_2} dy g(x, y)g(x + \Delta x, y + \Delta y) \right\rangle. \quad (\text{B.3})$$

C is given by the time-wise average of the autocorrelation function of the normalized granular intensity divided by the considered surface area. As stated before, C depends on distance alone so that one can further average the above expressions over circles $\Delta x^2 + \Delta y^2 = \text{const.}$, and obtain a one-dimensional function describing the decrease of correlation with increasing distance between two locations. In order to have our basic assumption fulfilled, the spatial scale over which the correlation drops should be significantly smaller than the linear patch size.

Here we have regarded the intensity, not the flux. However, since all inclinations follow roughly the same behavior, the correlation length of the intensities of all inclinations should be roughly the same. This implies a corresponding correlation length for the radiative flux.

References

- Abramowitz, M. & Stegun, I. 1972, Handbook of mathematical functions (Dover Publications)
- Aigrain, S., Favata, F., & Gilmore, G. 2004, A&A, 414, 1139
- Freytag, B. 2003, in Proceedings of the 12th Cambridge Workshop on Cool Stars, Stellar Systems, and the Sun, ed. A. Brown, G. Harper, & T. Ayres, 1024–1029
- Freytag, B., Holweger, H., Steffen, M., & Ludwig, H.-G. 1997, in Science with the VLT Interferometer, ed. F. Paresce (Springer), 316–317
- Green, D., Mathews, J., Seager, S., & Kuschnik, R. 2003, Astrophys. J., 597, 590
- Hatzes, A. 2002, Astron. Nachr., 323, 392
- Kjeldsen, H., Bedding, T., Frandsen, S., & Dall, T. 1999, MNRAS, 303, 579
- Lindgren, L. 1977, A&A, 57, 55
- Mathews, J., Kuschnik, R., Guenther, D., et al. 2004, Nature, 430, 51

- Steffen, M. & Freytag, B. 1995, Chaos, Solitons & Fractals, 5, no. 10, 1965
- Svensson, F. & Ludwig, H.-G. 2005, in Proceedings of the 13th Cambridge Workshop on Cool Stars, Stellar Systems, and the Sun (ESA SP-560), ed. F. Favata, G. Hussain, & B. Battrick (ESA Publications Division), 979–984
- Trampedach, R., Christensen-Dalsgaard, J., Nordlund, Å., & Stein, R. 1998, in The First MONS Workshop: Science with a Small Space Telescope, ed. H. Kjeldsen & T. Bedding (Aarhus Universitet), 59
- Wedemeyer, S., Freytag, B., Steffen, M., Ludwig, H.-G., & Holweger, H. 2004, A&A, 414, 1121